Electron Microscopy

International Edition: DOI: 10.1002/anie.201502236
German Edition: DOI: 10.1002/ange.201502236

Direct Imaging of Octahedral Distortion in a Complex Molybdenum Vanadium Mixed Oxide**

*Thomas Lunkenbein, Frank Girgsdies, Anna Wernbacher, Johannes Noack, Gudrun Auffermann, Akira Yasuhara, Achim Klein-Hoffmann, Wataru Ueda, Maik Eichelbaum, Annette Trunschke, Robert Schlögl, and Marc G. Willinger**

Abstract: *Complex Mo,V-based mixed oxides that crystallize in the orthorhombic M1-type structure are promising candidates for the selective oxidation of small alkanes. The oxygen sublattice of such a complex oxide has been studied by annular bright field scanning transmission electron microscopy. The recorded micrographs directly display the local distortion in the metal oxygen octahedra. From the degree of distortion we are able to draw conclusions on the distribution of oxidation states in the cation columns at different sites. The results are supported by X-ray diffraction and electron paramagnetic resonance measurements that provide integral details about the crystal structure and spin coupling, respectively.*

In the past 25 years, high-resolution transmission electron microscopy (HRTEM) has been developed to a powerful tool for direct imaging of atomic structures.[1] However, direct imaging of elements with low atomic number, such as oxygen, nitrogen, and hydrogen is difficult due to their low scattering power. For instance, in high-angle annular dark field scanning transmission electron microscopy (HAADF-STEM) the intensity is due to Rutherford scattering by the nuclei and, therefore, approximately proportional to Z^2.[2] As a result, the intensity of heavy elements generally overwhelms the signal of light ones. Nonetheless, individual oxygen columns have been observed by advanced techniques, such as exit wave reconstruction,[3] spherical aberration corrected TEM,[4] and high voltage HRTEM.[5] Although these methods show concepts to pinpoint the oxygen columns, their utilization is limited.

Pioneering work on the direct imaging of oxygen columns was mainly accomplished on structures derived from thermodynamically stable, high-temperature perovskites characterized by negligible beam sensitivity.[4b,5] In catalysis and energy conversion, however, metastable and specifically beam-sensitive phases exhibiting defects and distortions in the metal–oxygen polyhedra are generally used. Direct imaging of light elements in beam-sensitive materials is, however, possible by using an annular bright field (ABF) detector[6] in combination with STEM. Small-angle scattering occurs at the edge of the atoms where all elements have comparable charge densities. Thus the scattering intensities of light and heavy elements are more balanced.[7] Here we present the direct imaging of the oxygen sublattice in beam-sensitive, binary orthorhombic $(Mo,V)O_x$. Images were recorded with a double corrected JEOL ARM 200F equipped with a cold field emission gun (CFEG) using HAADF and ABF detectors.

$(Mo,V)O_x$ crystallizes in an orthorhombic structure (Pba2) closely related to the so-called M1 phase of $MoVTeNbO_x$ (ICSD no. 55097, Figure 1).[8] It has been considered as catalyst in the oxidative activation of short-chain alkanes in the light of prospected raw material changes from crude oil to natural gas.[9] The obtained ABF-STEM images enable a direct measurement of the metal–oxygen bond angles for the different metal sites. Although the measured distortions correspond to a projection onto the basal plane, they give a hint on the oxidation state of each metal site.[10] Our findings are compared with Rietveld refined X-ray diffraction (XRD) data and electron paramagnetic resonance (EPR) spectroscopy.

Aberration-corrected HAADF-STEM imaging has been used before[2,11] to directly observe the characteristic metal framework of the orthorhombic $(Mo,V)O_x$ structure in the [001] projection. It provided valuable insights on different metal site occupancies and defect structures.[2,12] In the case of highly crystalline $(Mo,V)O_x$ (Figure SI1), the analysis of HAADF images (Figure 2 A) showed a similar trend in the Mo site occupancy (Figure SI2). Using the labeling scheme suggested by DeSanto[8] et al., the Mo content in the respective sites decreases in the order $S9 \approx S5 \approx S6 > S8 \approx S10 \approx S11 > S2 > S4 \approx S3 \approx S7 > S1$. This result is in good agreement with the preferential positions of Mo and V obtained by Rietveld refinement of the XRD data (Figure 1, Table 1, and Table SI1). However, occupancies diverge slightly from observations reported previously, thus indicating

[*] Dr. T. Lunkenbein, Dr. F. Girgsdies, A. Wernbacher, Dr. J. Noack, A. Klein-Hoffmann, Dr. M. Eichelbaum, Dr. A. Trunschke, Prof. R. Schlögl, Dr. M. G. Willinger
Department of Inorganic Chemistry
Fritz-Haber-Institut der Max-Planck-Gesellschaft
Faradayweg 4–6, 14195 Berlin (Germany)
E-mail: willinger@fhi-berlin.mpg.de
Dr. G. Auffermann
Max Planck Institut für Chemische Physik Fester Stoffe
Nöthnitzer Straße 40, 01187 Dresden (Germany)
A. Yasuhara
Jeol Ltd.
Tokyo (Japan)
Prof. W. Ueda
Catalysis Research Center, Hokkaido University
Sapporo (Japan)
Prof. R. Schlögl, Dr. M. G. Willinger
Max-Planck-Institut für Chemische Energiekonversion
Stiftstrasse 34–36, 45470 Mülheim an der Ruhr, Germany

[**] J.N. thanks BasCat for a fellowship.
Supporting information for this article is available on the WWW under http://dx.doi.org/10.1002/anie.201502236.

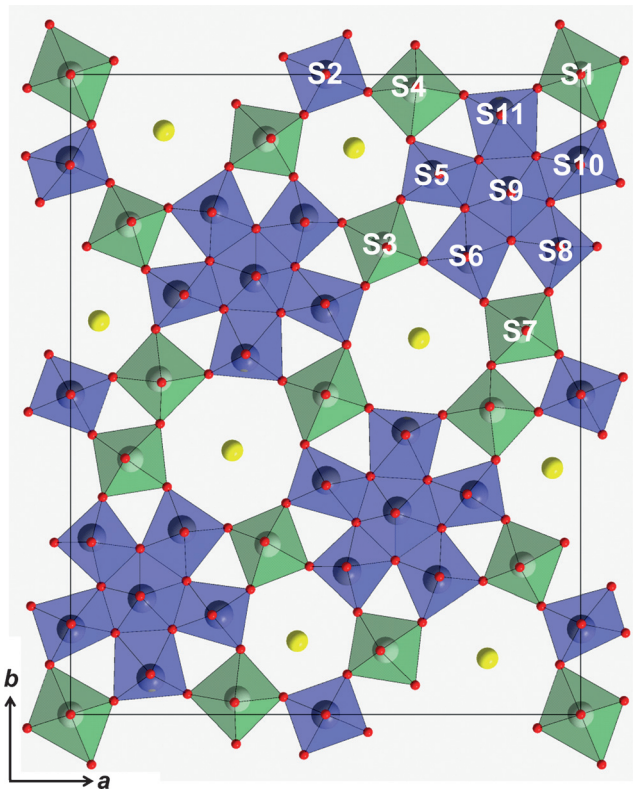

Figure 1. Polyhedron model of the orthorhombic (Mo,V)O_x structure viewed along [001] obtained from Rietveld refined XRD pattern (Figures SI4 and SI5). Mo- or V-dominated, channel and oxygen sites are denoted by blue or green polyhedra/atoms, yellow and red atoms, respectively.

Table 1: Measured oxygen-metal-oxygen bond angles within the basal plane of a low, medium, and high distorted metal site, preferred metal site occupation, and proposed oxidation states of Mo and V in the orthorhombic (Mo,V)O_x structure. Additional bond angles for various metal sites are listed in the Supporting Information (Table SI1).

Oxygen site[a]	Metal site	Oxygen site[a]	Bond angle [°][b]	Metal[c]	Population [at.%][d]	d^1 (OS)[e]
O26	S1	O13	90[f]	V	87	high
O13	S1	O26′	90 ± 1			(4+)
O26′	S1	O13′	90[f]			
O13′	S1	O26	90 ± 1			
O30	S3	O17	88 ± 4	V	69	low
O17	S3	O14	97 ± 3			(5+)
O14	S3	O15	89 ± 4			
O15	S3	O30	85 ± 3			
O19	S5	O30	109 ± 2	Mo	90	low
O30	S5	O18	83 ± 4			(6+)
O18	S5	O22	73 ± 4			
O22	S5	O19	95 ± 4			

[a] An oxygen site map is given in the Supporting Information (Figure SI11). [b] Measured metal–oxygen bond angles in the basal plane. Given numbers are averages of different spots. [c] Preferred metal at the corresponding metal site as determined from the XRD data (Figures 1 and SI5) and HAADF-STEM image (Figures 2A and SI2). [d] Occupancy of the dominating metal as obtained from XRD. The difference to 100% corresponds to the minor element. [e] Probability of realizing a d^1 state and proposed oxidation state. [f] Symmetry centers: The angle of neighboring metal–oxygen bonds has to be 180°.

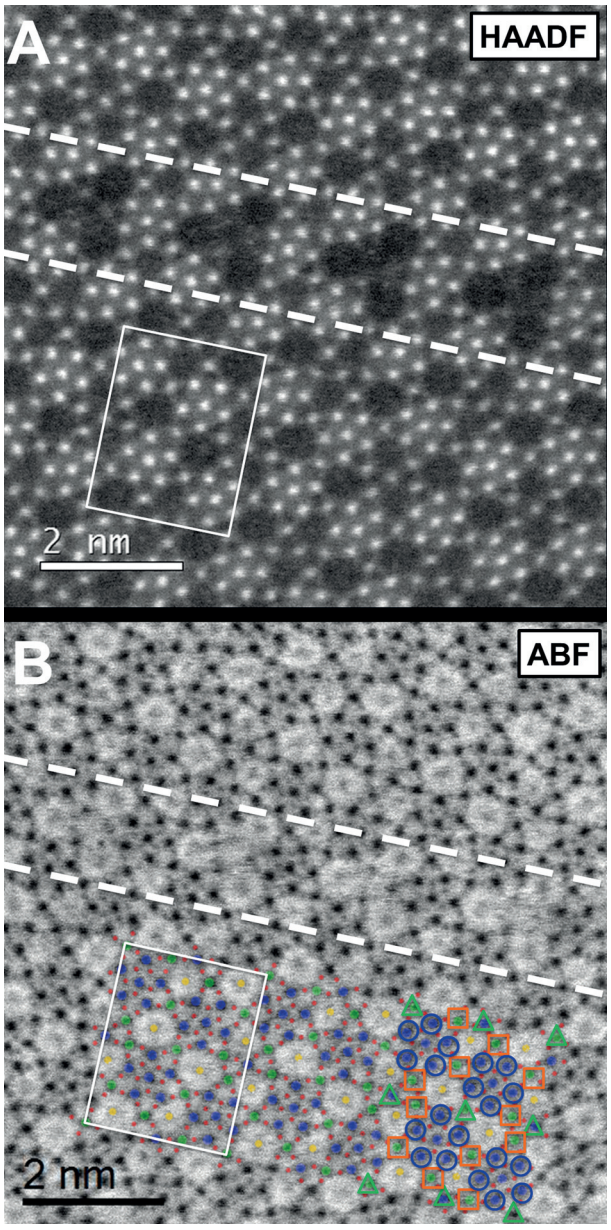

Figure 2. A) Atomic resolution HAADF-STEM image and simultaneously recorded ABF-image (B) of (Mo,V)O_x. The white rectangles in (A) and (B) display the orthorhombic unit cell. The white dashed lines in (A) and (B) denote a trigonal intergrowth. In (B) Mo-, V-dominating metal, channel, and oxygen sites are highlighted in blue, green, yellow, and red, respectively. In addition, metal sites with high, intermediate, and no distortions are indicated by blue circles, orange squares, and green triangles, respectively. Original ABF images are given in the Supporting Information (Figures SI7 and SI8).

a certain chemical flexibility of orthorhombic (Mo,V)O_x. Variations in the Mo and V distribution could be related to the fact that thermal treatment after hydrothermal synthesis was omitted. It is important to note here that STEM is a very local method and therefore allows resolving statistic occupation of inequivalent sites for individual unit cells (Figure SI3), whereas XRD averages over the whole sample.

The simultaneously recorded annular bright field (ABF)-STEM image is depicted in Figure 2B. In ABF, channels

appear bright, whereas individual metal and oxygen sites appear dark. As opposed to HAADF, the oxygen columns in the vicinity of the metal sites can clearly be observed in the ABF images. In agreement with the XRD measurements (Figures 1, SI4, and SI5), ABF shows that heptagonal[14] and hexagonal channels exhibit additional electron density indicating at least a partial occupancy of both channels. Interestingly, the highly localized contrast due to the oxygen columns indicates a relative confined distribution of O atoms, suggesting an equal distortion of the MO_6 octahedra stacks along [001] columns, regardless of the mixed Mo/V ratio. If the distortion at one site would vary, a diffuse contrast of the oxygen atoms would be expected. The direct imaging of the metal oxygen polyhedra provides information about bond angles that can otherwise only be obtained by a combination of different physical methods. However, direct measurement of structural parameters requires distortion-free imaging. To validate the absence of scan distortions a Pt reference sample was investigated using the same settings (see Figure SI6). Improved room design and the high stability of modern TEM platforms allow distortion-free imaging and abstraction of structural parameters as demonstrated in several recent publications.[15] The STEM images in Figure 2 and the measured angles correspond to a 2D projection of $(Mo,V)O_x$. Thus, the apical M−O bonds are not accessible. The measured bond angles of the different metal sites in $(Mo,V)O_x$ are listed in Tables 1 and SI1 and are schematically illustrated in Figure 2B. Almost no distortion was obtained in the basal plane of the S1 and S2 sites, medium distortions were measured at the S3, S4, and S7 sites, and the highest distortions were observed for the metal sites S5, S6, S8, S9, S10, and S11, which are located in the pentagonal units.

The distortion in transition metal oxides is a result of symmetry breaking due to energy minimization and depends on the spin configuration of the central cation[10] and the local surrounding.[16] Fully oxidized polyhedra consisting of Mo or V are known to always show a high out-of-center distortion tendency toward various directions[8,10] due to their ability to form stable "molybdenyl" or "vanadyl" (M = O; M = Mo,V) species. Structurally, the M1 phase represents a group of nonstoichiometric oxides such as Mo_5O_{14}, Mo_8O_{23}, and $Mo_{17}O_{47}$.[17] Mo_8O_{23} for instance also exhibits a complex framework, composed of distorted edge-shared octahedra hosting Mo=O species and less distorted bands of corner-shared polyhedra.[18] In the case of vanadium, V^{5+} polyhedra are generally distorted through one shortened bond length forming the characteristic V=O bond.[10b,19] While the strong distortion in highly oxidized Mo generally arises from a shortening of two metal oxygen bonds, in vanadium only one bond is compressed.[18,19] It has further been highlighted that the majority of Mo^{6+} cations tend to shift toward edges of the corresponding octahedra,[10b] leading to the occurrence of significant changes in the projected metal–oxygen bond angles. In the case of fully oxidized V, the metal centers are known to be mostly shifted toward the vertices,[10b] thus resulting in lower projected bond distortions. This is reflected in our measured metal–oxygen bond angles which are highest for the molybdenum oxide octahedra (Tables 1 and SI1) in the pentagonal building block.

Based on the measured projected distortions we therefore propose that medium and highly distorted sites (S3, S4, S7, S5, S6, S8, S10, and S11) contain empty d-orbitals and accommodate highly charged V and Mo cations, respectively. In contrast, almost no distortions are observed for symmetric S1 and S2 sites. Thus, these sites might exhibit an increased probability for hosting one d-electron at the respective metal centers. Finally, in the case of the pentagonal bipyramidal S9 site, no strong distortions were observed, although XRD data and HAADF-STEM analysis indicate that it is mainly occupied by Mo (Figure 2B, Table 1) and, according to charge neutrality, should be in a d^0 oxidation state. Hence, we cannot draw conclusions on the relation between distortion and d-occupancy in the case of the pentagonal bipyramid.

To verify the presence of unpaired electrons an EPR measurement was conducted. The corresponding spectrum (Figure SI9) can be fitted by two broad featureless signals and two signals containing hyperfine splitting (Figure SI10). The g-factors for the broad signals are typical for strongly interacting V (or Mo) species with 3d (or 4d) electrons. These features are indicating the presence of two distinguishable metal sites in the bulk phase and were therefore used for correlation. The signals with resolved hyperfine structure correspond to isolated $^{51}V^{4+}$ in an axial crystal field. Quantification of the spin numbers in the sample under the assumption that only d^0 and d^1 cations are present, reveals that at least 1–2% of the metals carry unpaired d-electrons (Tables SI2–SI5). In line with our assignment, the results could be translated to the presence of d^1 electrons at the S1 and S2 site. It should be mentioned that the EPR-detected amount of unpaired electrons represents a minimum value for d^1 electrons present in the unit cell of $(Mo,V)O_x$.

Our assignments of the metal site occupancy, distortion in the oxygen sublattice and oxidation state based on STEM micrographs are in very good agreement with XRD and EPR measurements. The combination of edge- and corner-shared M–O polyhedra (M = Mo, V) with different degrees of distortion relieve lattice strain and lead to the realization of this energetically favored, complex network structure. Such structures can be obtained by Mo or V because they are able to form discrete molybdenyl (Mo=O) and vanadyl (V=O) species, respectively. As the distortions are also affected by the electronic configuration, imaging of distortions in the oxygen sublattice enables a way to conclude on the oxidation state. The knowledge of the oxidation state of each single metal site will contribute to a better understanding of the redox chemistry of these materials and their function as prospective catalysts. Contrary to the HAADF-STEM image which gives the impression of empty channels which cannot be found by gas adsorption, the ABF image shows occupied channels. This result further underlines the power of modern chemical TEMs equipped with an ABF detector to verify the filling of nominal channels in inorganic structures. This report demonstrates that we are getting closer to Feynman's wish of understanding the atomic arrangement by just looking at it.

In conclusion, we have demonstrated that modern electron microscopy provides detailed chemical information that could otherwise only be obtained by a combination of

different analytical methods and could therefore be labeled as chemical electron microscopy (ChemEM). Abstracting local oxidation states from the atomic position in images provides an alternative to electron energy loss spectrometry for cases of beam-sensitive materials.

Experimental Section

The (Mo,V) oxide (FHI-SN: 11345) was prepared by hydrothermal synthesis and analyzed without further thermal treatment.[14] Details regarding synthesis and the applied analytical techniques are summarized in the Supporting Information.

Keywords: annular bright field microscopy · bond angles · electron microscopy · light elements · transmission electron microscopy

How to cite: *Angew. Chem. Int. Ed.* **2015**, *54*, 6828–6831
Angew. Chem. **2015**, *127*, 6932–6935

[1] a) K. W. Urban, *Nat. Mater.* **2009**, *8*, 260–262; b) M. Haider, S. Uhlemann, E. Schwan, H. Rose, B. Kabius, K. Urban, *Nature* **1998**, *392*, 768–769; c) P. E. Batson, N. Dellby, O. L. Krivanek, *Nature* **2002**, *418*, 617–620.
[2] W. D. Pyrz, D. A. Blom, M. Sadakane, K. Kodato, W. Ueda, T. Vogt, D. J. Buttrey, *Chem. Mater.* **2010**, *22*, 2033–2040.
[3] a) C. Kisielowski, C. J. D. Hetherington, Y. C. Wang, R. Kilaas, M. A. O'Keefe, A. Thust, *Ultramicroscopy* **2001**, *89*, 243–263; b) K. Yoshida, T. Kawai, T. Nambara, S. Tanemura, K. Saitoh, N. Tanaka, *Nanotechnology* **2006**, *17*, 3944.
[4] a) C.-L. Jia, S.-B. Mi, K. Urban, I. Vrejoiu, M. Alexe, D. Hesse, *Nat. Mater.* **2008**, *7*, 57–61; b) C. L. Jia, M. Lentzen, K. Urban, *Science* **2003**, *299*, 870–873.
[5] Z. Zhang, W. Sigle, F. Phillipp, M. Rühle, *Science* **2003**, *302*, 846–849.
[6] W. O. Saxton, W. K. Jenkins, L. A. Freeman, D. J. Smith, *Optik* **1978**, *49*, 505–510.
[7] P. E. Batson, *Nat. Mater.* **2011**, *10*, 270–271.
[8] P. DeSanto, J. Buttrey Douglas, K. Grasselli Robert, G. Lugmair Claus, F. Volpe Anthony, H. Toby Brian, T. Vogt, *Z. Kristallogr.* **2004**, *219*, 152.
[9] T. Konya, T. Katou, T. Murayama, S. Ishikawa, M. Sadakane, D. Buttrey, W. Ueda, *Catal. Sci. Technol.* **2013**, *3*, 380–387.
[10] a) M. Kunz, I. D. Brown, *J. Solid State Chem.* **1995**, *115*, 395–406; b) K. M. Ok, P. S. Halasyamani, D. Casanova, M. Llunell, P. Alemany, S. Alvarez, *Chem. Mater.* **2006**, *18*, 3176–3183.
[11] W. D. Pyrz, D. A. Blom, T. Vogt, D. J. Buttrey, *Angew. Chem. Int. Ed.* **2008**, *47*, 2788–2791; *Angew. Chem.* **2008**, *120*, 2830–2833.
[12] W. D. Pyrz, D. A. Blom, M. Sadakane, K. Kodato, W. Ueda, T. Vogt, D. J. Buttrey, *Proc. Natl. Acad. Sci. USA* **2010**, *107*, 6152–6157.
[13] E. J. Kirkland, *Advanced Computing in Electron Microscopy*, Springer, New York, **2010**.
[14] S. Ishikawa, T. Murayama, S. Ohmura, M. Sadakane, W. Ueda, *Chem. Mater.* **2013**, *25*, 2211–2219.
[15] a) I. MacLaren, Q. M. Ramasse, *Int. Mater. Rev.* **2014**, *59*, 115–131; b) X. Li, X. Ma, D. Su, L. Liu, R. Chisnell, S. P. Ong, H. Chen, A. Toumar, J.-C. Idrobo, Y. Lei, J. Bai, F. Wang, J. W. Lynn, Y. S. Lee, G. Ceder, *Nat. Mater.* **2014**, *13*, 586–592.
[16] K. Amakawa, L. Sun, C. Guo, M. Hävecker, P. Kube, I. E. Wachs, S. Lwin, A. I. Frenkel, A. Patlolla, K. Hermann, R. Schlögl, A. Trunschke, *Angew. Chem. Int. Ed.* **2013**, *52*, 13553–13557; *Angew. Chem.* **2013**, *125*, 13796–13800.
[17] L. Kihlborg in *Nonstoichiometric Compounds*, *Vol. 39*, American Chemical Society, Washington, DC, **1963**, pp. 37–45.
[18] E. Canadell, M. H. Whangbo, *Inorg. Chem.* **1990**, *29*, 2256–2260.
[19] H. Björk, S. Lidin, T. Gustafsson, J. O. Thomas, *Acta Crystallogr. Sect. B* **2001**, *57*, 759–765.

Received: March 10, 2015
Published online: April 27, 2015

